International Journal of Engineering Trends and Technology
ISSN: 2231–5381 / https://doi.org/10.14445/22315381/IJETT-V71I9P224

Volume 71 Issue 9, 265-281, September 2023

Original Article

Grid Incorporated PV System with SBQZS Converter Controlled using Optimization Techniques

P.K. Dhal[1], K. Barathi[2]

[1,2]*Department of Electrical and Electronics Engineering, Vel Tech Rangarajan Dr.Sagunthala R&D Institute of Science and Technology, Tamil Nadu, India*

[1]*Corresponding Author : pradyumna.dhal@rediffmail.com*

Received: 01 January 2023 Revised: 18 June 2023 Accepted: 17 August 2023 Published: 03 September 2023

Abstract *- The increasing depletion of fossil fuels combined with global warming and climate variation has necessitated the development and high-level infusion of Renewable Energy Sources (RES) to electric power systems. Among these RESs, the Photovoltaic (PV) system that transforms solar power into electricity is easily accessible with huge untapped potential. The interfacing of the PV system to the load/grid requires the application of a high-gain converter. So, a high gain Switched Boost Quasi Z-Source (SBQZS) converter is proposed with a maximum gain of 1:10. The proposed converter is effective in overcoming the limitations of conventional converters in enhancing the reliability and efficiency of the system by improving the current profile and reducing the voltage stress. The converter control is accomplished by a PI controller, the parameters of which are tuned using optimization algorithms like Particle Swarm Optimization (PSO), Artificial Bee Colony (ABC), and Chicken Swarm (CS) and their performances are analogized. The performance of the proposed configuration is analyzed by simulation in MATLAB and hardware by FPGA Spartan 6E, which results in a maximum efficiency of* 97% *and minimizes THD.*

Keywords *- PV system, Particle Swarm Optimization, Artificial Bee Colony, Chicken Swarm Algorithm, Grid Synchronization, SBQZS.*

1. Introduction

As the energy demand is increasing day by day, it is crucial to conserve energy, and the usage of RES is the way to energy conservation. The phenomena of global warming and its detrimental impact on the environment have also resulted in the need to develop RES, which provides clean energy with reduced emissions. Renewable energy sources with electrical grid networks are integrated by utilizing power electronics technology; they also play a prominent role in distributed generation [1-3]. Generally, smart grids are characterized as stand-alone and grid-connected types; anyway, the majority of PV systems are coupled with the grid [4]. The power plant industry is experiencing a rapid enhancement, with the capacity reaching hundreds of megawatts. This growth has led to a significant extension of grid-connected PV inverters, particularly in large-scale installations, garnering considerable attention. The deployment of these extensive PV inverters varies based on the country's energy usage patterns and the characteristics of the connected grids, where they are predominantly associated with either Low Voltage (LV) or Medium Voltage (MV) grids. These adaptations are essential to cater to diverse grid requirements and ensure efficient integration of solar power into the existing energy infrastructure. [5-6]. Grid-connected PV systems inject power directly into the grid, and solar generation variability can cause grid voltage and frequency fluctuations. In certain scenarios, this may affect the grid's stability, particularly if there is a high penetration of solar energy. High levels of PV generation during peak solar periods can lead to increased voltage levels in the grid. Voltage regulation is necessary to avoid overvoltage conditions that damage equipment and affect other connected devices. To ensure smooth integration with the grid, PV systems need to be synchronized with the grid's frequency and phase. If not properly synchronized, the power injection into the grid can cause disruptions and disturbances. The primary objective is to optimize the utilization of solar power generated by the PV panel. A current control scheme is employed to achieve this, allowing the extreme active power produced in the PV array to be directly supplied to the grid. This approach ensures stability in power systems connected to both low-voltage and medium-voltage grids. However, there are some limitations in its execution. One such weakness is the power consumption fluctuation due to grid voltage and frequency variations. The grid frequency is influenced by the speed at which the power is supplied, leading to variable power consumption patterns. Addressing these issues is crucial to increase the overall performance of the system and further promote efficient utilization of solar

energy [7-9]. The maximum penetration of RES causes grid instability; to overcome this, active power control through grid frequency variation is performed [10]. However, the current control scheme does not control the variation in grid voltage; to prevent this, reactive power is supplied through the grid-connected PV inverter. Hence, effective grid synchronization must be accomplished, providing active and reactive power compensation with reduced THD.

To boost the outcome of PV, converters are utilized that perform low DC voltage to high DC voltage conversion. Some of the utilized converters of PV systems are Boost converters, SEPIC converters, LUO converters and Z-source converters. Among these converters, Boost converters are used initially and are also stated as step-up converters. The converter generates an output voltage that exceeds the supply voltage. However, it comes with the drawback of having low efficiency, resulting in a failure to achieve significant gains. [11].

To address the challenges posed by the boost converter, the buck-boost converter [12] is employed. This converter enables the generation of DC voltages within various ranges. However, one limitation of this approach is that the continuous flow of current can lead to damage to the converter. To overcome these challenges, a SEPIC converter [13] is exploited. This converter employs a single-duty cycle to regulate the generated DC voltage, which can be lower than, equal to, or higher than the supply voltage. Additionally, the input current supplied to this converter remains continuous. Nevertheless, it should be noted that the SEPIC converter is unsuitable for applications with low variability in voltage [14].

The limitations of the SEPIC converter are effectively addressed by the CUK converter. This converter allows for generating different voltage ranges with high static gain, ensuring a constant DC supply. However, it necessitates a significant number of components for storage and can lead to high current stress [15, 16]. To tackle these challenges, the Z-source converter is implemented. It is known for its unique impedance network that couples the main circuit and power sources [17]. The Z-source converter operates in either boost or buck-boost mode, enabling it to overcome the drawbacks of the previous converters. Despite its advantages, one downside of this converter is its relatively lower reliability compared to other solutions [18]. Considering the above-discussed factors, a novel SBQZS converter is proposed, which is a combination of Boost and Quasi Z-source converters.

Generally, for PV systems to extricate maximum power, Maximum Power Point Tracking (MPPT) has been engaged [19]. Several techniques perform MPPT, and the P&O (Perturb and Observe) algorithm is one among them; by this, the MPP tracking is performed, which causes variations in the PV module [20]. It also evaluates the output PV power and compares it with the previous value, and due to the atmospheric conditions, MPP is deviated [21]. The incremental conductance method is employed to address the issue, ensuring that the rate of PV current variation matches the PV voltage changes [22]. However, this algorithm may not perform optimally under conditions of significant variations in insolation [23]. Alternatively, a fuzzy logic controller is exploited in nonlinear PV systems for tracking maximum power without relying on precise system data [24].

Nevertheless, the fuzzy logic approach lacks adaptivity when dealing with different operating points of the PV system [25]. Although MPPT techniques are adopted in grid-connected PV systems to optimize power generation, they may not completely eliminate fluctuations in the link voltage. Hence, in this work, the desired voltage is attained by implementing closed-loop control with a PI controller optimized by meta-heuristic algorithms. When compared to open-loop systems, the closed-loop system generates accurate and reliable results with the presence of a feedback loop.

In this work, an SBQZS converter is proposed for a grid-linked PV system, which ensures that the PV system's output voltage is appropriately adjusted to synchronize with the grid's voltage, allowing seamless integration of solar power into the electrical grid. To achieve precise control of the SBQZS converter, a PI controller relies on appropriately tuning its parameters. This work employs optimization techniques such as PSO, ABC and CS to tune the PI controller's parameters. Furthermore, the generated power is synchronized with the grid's frequency and phase using a PI controller. A detailed comparison and analysis of these optimization techniques are performed, and the corresponding performances are validated. The paper is ordered as follows: Proposed system configuration in section 2, modeling of proposed configuration in section 3, Control of Converter with Optimization Technique, technical details in section 4, 5, 6 Results and Discussions in section 7 and conclusion in section 8.

2. Proposed System Configuration

The proposed configuration of the PV unified grid is shown in Fig. 1, which displays the interconnection of PV with the grid in which DC-DC conversion and DC-AC conversions are carried out by means of the proposed SBQZS converter and 1ϕ Voltage Source Inverter (VSI), respectively.

The output of PV is applied to the SBQZS converter, the voltage-gain ratio of which is 1:10; thus, the converter boosts PV voltage by 10 times. The converter's output is tied to 1ϕ VSI, the outcome of which is fed to the grid.

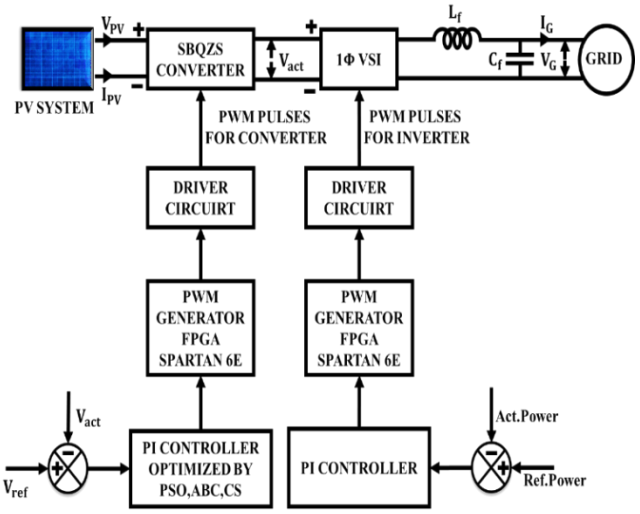

Fig. 1 Proposed system configuration

A PI controller with closed-loop control is suggested to retain the link voltage between VSI and the converter, and its output is applied to a PWM pulse generator. Because of the feedback signal of the closed-loop control, the outputs of the PI controller are accurate, maintaining the system's stability with constant link voltage. The PI controller relates reference and actual voltage values, and accordingly, reference output is provided by the PI controller. The input reference voltage of the comparator is selected as 300V, which indicates the rms value of the actual voltage.

Optimization approaches like PSO, ABC and CS are adopted to tune PI controller parameters. This generates optimized reference outputs, which are applied to the PWM generator. The PWM generator now analogizes the carrier signal with a reference signal, and accordingly, PWM pulses are produced to control the converter, thereby retaining the link voltage. While interconnecting the system with the grid, it is noted that certain imbalances are neutralized by the effect of the PI controller with closed-loop control utilized on the grid side. Thus, the reactive power compensation is achieved, thereby attaining maximum efficiency and minimum THD.

3. Proposed Configuration Modeling

3.1. Grid-Tied PV System Model

A grid-coupled PV system is adopted in which a PV array is linked to the utility grid via an inverter. It includes a ripple filter (C_f, R_f), interfacing inductor (L_i, R_i) as indicated in Fig.2. The switching ripples generated by VSI are eliminated by the ripple filter.

The solar cell is considered a crucial component of a PV array. The PV module is designed by multiple individual PV cells linked in series. The PV system's equivalent circuit is described in Fig. 3. This circuit comprises photocurrent (I_{ph}), series resistance (R_s), Diode (D) and shunt resistance (R_{sh}).

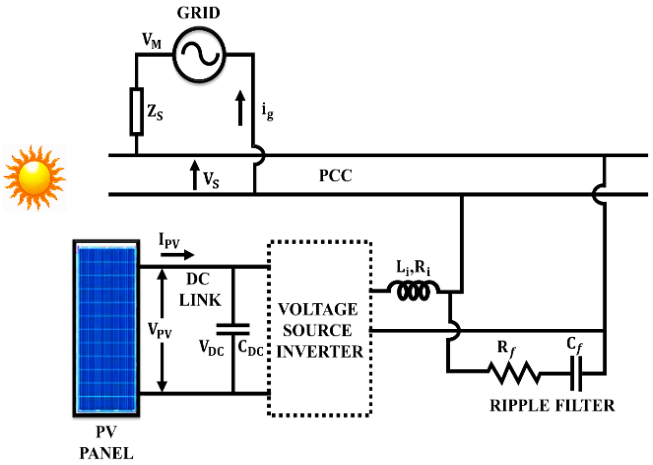

Fig. 2 Grid-tied PV system

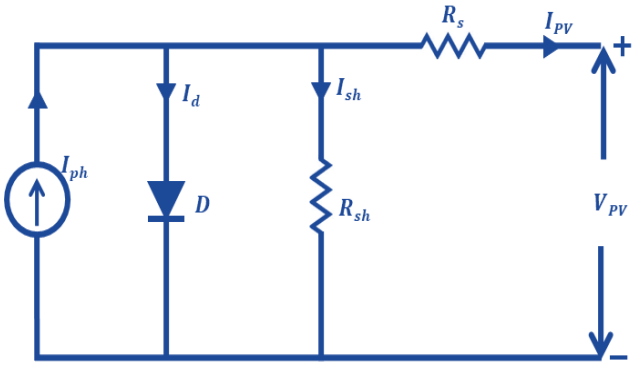

Fig. 3 Equivalent circuit of PV system

The relationship between the output voltage and current is expressed as

$$,I_{PV} = I_{ph} - I_{sh}\left(exp\left(\frac{V_{PV}+IR_S}{AN_S kT}\right) - 1\right) - \frac{V_{PV}+IR_S}{R_{sh}} \quad (1)$$

where the photocurrent is specified as I_{ph}, saturation current is termed as I_{sh}, ideal diode factor is denoted as A, the electron charge is denoted as $q = 1.602 \times 10^{-19}\ C$, Boltzmann's constant is denoted as $k = 1.381 \times 10^{-23}$, the cell temperature is denoted as T and the number of PV cells linked in series is denoted as N_s.

At any temperature and solar irradiation, the photocurrent of the PV cell is expressed as,

$$I_{ph} = \frac{G}{G_{ref}}[I_{sc} + K_i(T - T_{rk})] \quad (2)$$

$$\mathrm{I_{sc}} = \mathrm{I_{sc,ref}}\left(\frac{\mathrm{R_p}+\mathrm{R_s}}{\mathrm{R_p}}\right) \quad (3)$$

$$\mathrm{I_{sat}} = \frac{\mathrm{I_{SC,ref}}+\mathrm{K_i}(\mathrm{T}-\mathrm{T_{rk}})}{\mathrm{e^q}\left(\mathrm{V_{oc,ref}}+\frac{\mathrm{k_V}(\mathrm{T}-\mathrm{T_{rk}})}{\mathrm{AN_S kT}}\right)-1} \quad (4)$$

Here, the reference and actual solar irradiation are denoted as G_{ref} *and* G respectively, module absolute

temperature (K) is denoted as T_{rk}, the temperature coefficient is denoted as K_i and k_v, short circuit current and open circuit voltage at reference condition is denoted as $I_{SC,ref}$ and $V_{oc,ref}$. The outcome of PV is fed to the converter to get the desired link voltage.

3.2. Switched Boost Quasi-Z source (SBQZS) Converter

This converter is an arrangement of a quasi-Z-source and a boost converter with a voltage gain of 1:10. The quasi-Z-source converter possesses buck-boost characteristics and accomplishes single-stage power conversion. The boost converters adopt a shoot-through state for enhancing the voltage, but the boost factor is comparatively low. Hence, the boost converter is combined with a quasi-Z-source converter, generating an improved current profile and reduced voltage stress. The overall combination increases the efficiency and reliability of the system. The representation of the SBQZS converter is explained in Fig. 4, which comprises three diodes (D_1, D_2, D_o), four capacitors(C_1, C_2, C_3, C_o), two inductors (L_1, L_2) with one switch(S). The diode D_1 restricts the current flow back to the PV system. For the converter analysis in steady state, some presumptions are made as follows: All the diodes, capacitors and inductors are considered ideal, ignoring the parasitic effect. So $L_1 = L_2 = L$ and $C_1 = C_2 = C_3 = C$.

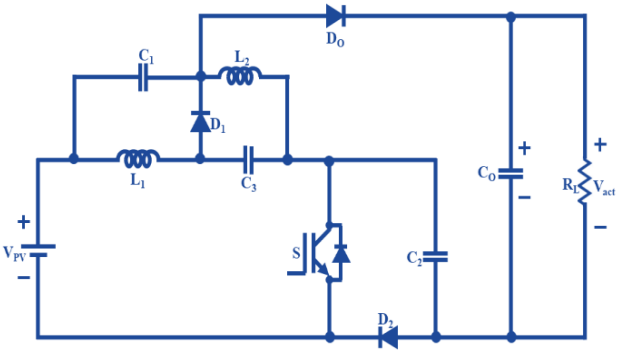

Fig. 4 Schematic representation of SBQZS converter

The two operating modes of the converter are elaborated as follows:

3.2.1 Mode 1 Operation

The illustration of the mode 1 operation of the SBQZS converter is given in Fig. 5 (a). During this mode, S, D_o is in ON condition with D_1, D_2 in the OFF condition, this is because the diodes are in reverse and are connected to the capacitors in a parallel manner. The inductance L_1 gets charged by V_{PV} and C_3 while L_2 gets charged by V_{PV}, and C_1. As C_1 and C_2 are coupled in series with V_{PV}, the load is supplied by means of the switch. In mode 1, the steady-state equation for the converter is estimated by applying KVL,

$$\begin{cases} V_{L_1} = V_{PV} + V_{C_3} \\ V_{act} = V_{PV} + V_{C_1} + V_{C_2} \end{cases} \quad (5)$$

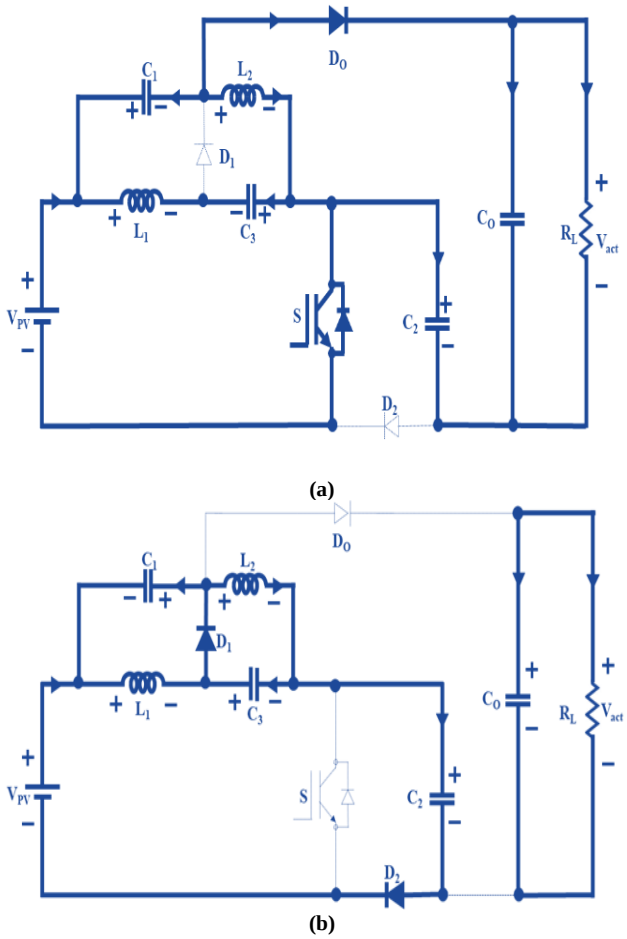

Fig. 5 SBQZS converter operation (a) Mode 1 (b) Mode 2

3.2.2. Mode 2 Operation

The illustration of the mode 2 operation of the SBQZS converter is depicted in Fig. 5 (b). During this mode, D_1, D_2 is in ON condition, and S is in OFF condition while the diode D_o is reverse blocking. C_1 gets charged by L_1; C_3 gets charged by L_2; C_2 gets charged by V_{PV} and L_1; R_L is energized by C_o. In mode 2, the steady-state equation for the converter is estimated by applying KVL,

$$\begin{cases} V_{L_1} + V_{C_1} = 0 \\ V_{L_2} + V_{C_3} = 0 \\ V_{PV} = V_{L_1} - V_{C_3} + V_{C_2} \end{cases} \quad (6)$$

In steady-state, the average voltage through the inductor becomes zero, and this is because of the volt-second balance behavior of the inductor. The duty cycle is given as,

$$D = \frac{T_{on}}{T_s} \quad (7)$$

Here, the conduction time is denoted by T_{on} and its respective switching period is denoted as T_s.

$$V_{C_1} = V_{C_3} = \frac{D}{1-2D} V_{PV} \quad (8)$$

$$V_{C_2} = V_{PV} + V_{C_1} + V_{C_3} = \frac{1}{1-2D} V_{PV} \quad (9)$$

The output voltage of the converter V_{act} is estimated with equations (4) and (5),

$$V_{C_2} = V_{PV} + V_{C_1} + V_{C_3} = \frac{1}{1-2D} V_{PV} \quad (10)$$

Thus, the voltage gain of the SBQZS converter is given as,

$$G = \frac{V_{act}}{V_{PV}} = \frac{2-D}{1-2D} \quad (11)$$

3.2.3. Selection of Parameters

The voltage and current stress play a vital role in selecting the parameters, as the rated current and voltage are the factors that rely on this.

Considering mode 1 operation, the voltage stress on the diodes (V_{D_1}, V_{D_2}) are given as,

$$V_{D_1} = V_{D_2} = \frac{1}{1-2D} V_{PV} \quad (12)$$

Considering mode 2 operation, the voltage stress on the diode (V_{D_o}) and switch (V_S) are given as,

$$V_S = V_{D_o} = \frac{1}{1-2D} V_{PV} \quad (13)$$

An assumption is made such that the inductor is large and the current through the inductor varies linearly. And so, the current through the inductor is given as

$$\begin{cases} I_{L_1} = \frac{2-D}{1-2D} I_o \\ I_{L_2} = \frac{1+D}{1-2D} I_o \end{cases} \quad (14)$$

For mode 1 operation (S-ON), the current through S and D_o are given as,

$$\begin{cases} I_S = \frac{1+D}{D(1-2D)} I_o \\ I_{D_o} = \frac{I_o}{D} \end{cases} \quad (15)$$

For mode 2 operation (S-OFF), the current through D_1 and D_2 are given as,

$$\begin{cases} I_{D_1} = \frac{2-D}{(1-D)(1-2D)} I_o \\ I_{D_2} = \frac{1}{1-D} I_o \end{cases} \quad (16)$$

Thus, the average value of current through S, D_1, D_2 are given as

$$\begin{cases} I_{D_1} = \frac{2-D}{1-2D} I_o \\ I_{D_2} = I_{D_o} = I_o \\ I_S = \frac{1+D}{1-2D} I_o \end{cases} \quad (17)$$

3.2.4. Selection of Inductors

During mode 2 operation (S-OFF), the value of inductors is given as,

$$L = \frac{V_L dt}{di_L} \quad (18)$$

Here, the ripple current through the inductor is denoted by di_L, the OFF-state duration is denoted by $dt = (1-D)T_S$. If the inductor is large, the stress across the switch and diode will also be high, so there arises a necessity to limit the ripple current. The allowed ripple range is denoted by x_L %.

$$d_{i_L} = \frac{V_L dt}{L} = x_L \% I_L \quad (19)$$

Considering mode 2 operation, the values of inductors are given as,

$$L_1 = \frac{(1-D)T_S V_{C_1}}{x_L \% I_{L_1}} \quad (20)$$

$$L_2 = \frac{(1-D)T_S V_{C_3}}{x_L \% I_{L_2}} \quad (21)$$

3.2.5. Selection of Capacitors

Like the inductor, the capacitor also exhibits a little variation, and the allowed range is denoted by x_C%.Considering mode 1 operation (S-ON), the capacitance is given as,

$$C = \frac{I_{Con} dt}{dV_C} \quad (22)$$

Here, the current through the capacitor (S-ON) is denoted by I_{Con}, ON time of the switch is given as $dt = DT_S$, and $dV_C = x_C \% V_C$. The value of capacitances is given as,

$$\begin{cases} C_1 = \frac{(D^2-D+1)I_o}{D x_C \% V_{PV} f_s} \\ C_2 = \frac{(1-2D)I_o}{x_C \% V_{PV} f_s} \\ C_3 = \frac{(2-D)I_o}{x_C \% V_{PV} f_s} \end{cases} \quad (23)$$

Considering mode 2 operation (S-OFF), D_o is reverse blocking, and so the current through C_o is same as I_o.

$$C_o = \frac{I_o dt}{\Delta V_{C_o}} = \frac{I_o dt}{x_C \% V_{act}} \quad (24)$$

Substituting $dt = (1-D)T_S$ in equation (20),

$$C_o = \frac{(1-D)(1-2D)I_o}{(2-D)x_C \% V_{PV} f_s} \quad (25)$$

The switch S is selected depending on the current and voltage stresses. The controller's working is realized only when the converter is under proper control, carried out by a PI controller, which also aids in retaining the link voltage.

4. Control of Converter with Optimization Technique

The tuning parameters like K_p and K_i are utilized for controlling the DC-link voltage of the PV-integrated systems. In real-time operation, the optimal configuration of PI parameters like K_p and K_i are utilized to attain the finest optimal solution, which minimizes the transient response, reduces maximum peak overshoot issues and minimizes steady state error owing to the disturbance of the load in the PV integrated system. In this paper, the tuning of the PI controller is carried out with optimization algorithms such as PSO, ABC and CSOA.

4.1. Particle Swarm Optimization Algorithm

On the basis of the normal performance of bird flocks and fish schools, the PSO algorithm is established. Each particle travels in the direction of the finest result found so far in the group at each iteration. Holding this in place, the particle proceeds to look for a superior solution to the preceding one and move to it by thoroughly exploring the field. The i^{th} particle of the swarm's position and velocity in the search space vector is expressed as $X_i = [X_{i1,}X_{i2,} \dots X_{iD,}]$ and $V_i = [V_{i1,}V_{i2,} \dots V_{iD,}]$ accordingly. The finest previous solution for i^{th} the particle of the swarm is $P_i = [P_{i1,}P_{i2,} \dots P_{iD,}]$ and global finest solution is $P_g = [P_{g1,}P_{g2,} \dots P_{gD,}]$. The simplified location and velocity of every particle is expressed as,

$$V_i^{n+1} = \omega V_i^n + C_1 r_1 (P_i^n - X_i^n) + C_2 r_2 (P_g^n - X_i^n) \quad (26)$$

$$X_i^{n+1} = X_i^n + V_i^{n+1} \quad (27)$$

Where $i = 1, 2, \dots, m$), iteration number is denoted as n, inertia weight is denoted as ω, social rate and cognitive rate are denoted as $C_1 and\ C_2$, random intervals $(0, 1)$ are denoted as $r_1 and\ r_2$.

In order to determine the link voltage and attain the finest result for every parameter in the complete group, the PSO algorithm performs random initialization. The steps mentioned by,

Step 1: Initialize variables like the number of populations (N), maximum number of iterations(I), weight coefficients (C_1, C_2), lower and upper bounds (LB, UB), velocity (V), number of variables (NV) and inertia coefficient (W).

Step 2: Set the lower and upper limits.

Step 3: Determine PI controller parameters and initialize the swarms as zero based on the number of variables(NV) and population number(N).

$$swarm = \text{zeros} \begin{bmatrix} X_{1,1} & X_{1,2} & \dots & X_{1,NV} \\ X_{2,1} & X_{2,2} & \dots & X_{2,NV} \\ \vdots & \vdots & \ddots & \vdots \\ X_{N,1} & X_{N,2} & \dots & X_{N,NV} \end{bmatrix} \quad (28)$$

Step 4: Initialize the swarm population. The group of population is generated at this step, the matrix of which equals $NV * N$, and calculated as,

Step 5:

$$X_{i,j} = \text{round}\left(LB_j + \text{rand}(0,1) * (UB_j - LB_j)\right) \quad (29)$$

$$i = 1, 2, \dots\dots, N, j = 1, 2, \dots\dots NV$$

The population vectors are initialized as,

$$\text{Swarm} = \begin{bmatrix} X_{1,1} & X_{1,2} & \dots & X_{1,NV} \\ X_{2,1} & X_{2,2} & \dots & X_{2,NV} \\ \vdots & \vdots & \ddots & \vdots \\ X_{N,1} & X_{N,2} & \dots & X_{N,NV} \end{bmatrix} \quad (30)$$

Every swarm uses its flies and memory over the search area to attain a superior location than its existing one.

Step 6: Enhance particle produced using novel swarm. In its particle, the finest experience is memorized, i.e., P_{best}along with a group of the best G_{best}. A novel swarm is produced, which is given below,

$$V_{i,j}{}^{t+1} = wV_{i,j}{}^t + C_1 rand[0,1]X\left(Pbest_{i,j}{}^t - X_{i,j}{}^t\right) + C_2 rand[0,1]X\left(Gbest_{i,j}{}^t - X_{i,j}{}^t\right) \quad (31)$$

The updated location is expressed as,

$$X_{i,j}{}^{t+1} = V_{i,j}{}^{t+1} + X_{i,j}{}^t \quad (32)$$

Step 7: The assessment of fitness has been conducted.

The novel vector is enhanced based on the rule mentioned above and assessed based on link voltage fitness. The updated global and personal best results are expressed as,

If $fitness\left(X_{i,j}{}^{t+1}\right) < fitness\left(Pbest_{i,j}{}^t\right)$ then (33)

end

If $\text{fitness}\left(\text{Pbest}_{i,j}{}^t\right) < \text{fitness}\ (\text{Gbest})$ *then,*

$\text{Gbest} = \text{Pbest}_{i,j}{}^t$ (34)

end

Step 8: Stop the program

If the number of iterations is raised, then optimization is terminated. Or else, carry on with steps 6 and 7.

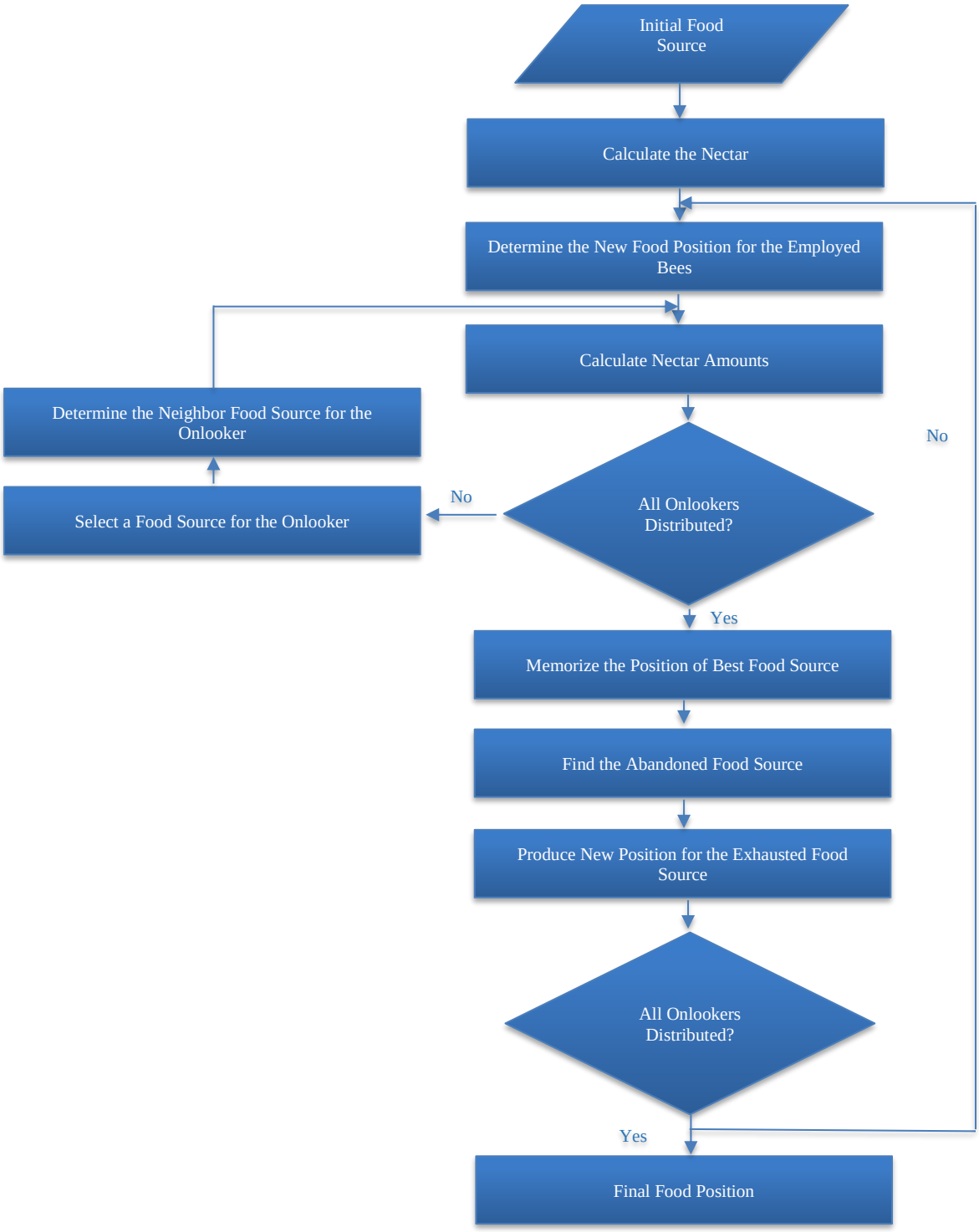

Fig. 6 ABC algorithm's flowchart

By this algorithm, the parameters of the PI controller have been tuned, and the link voltage is maintained.

PSO algorithm has a slow convergence rate and local minima problem; the ABC algorithm is utilized to overcome these disadvantages.

4.2. Artificial Bee Colony Algorithm

ABC Algorithm is used to overcome the slow convergence rate and local minima problem drawback. Also, it is implemented to control the PI parameters of K_p *and* K_i values. This algorithm was introduced by karaboga. This imitates the behaviors and intelligent foraging performance

of the group of honey bees when searching for food and sharing the quantity of food with other bees. Three classes of bees in the ABC algorithm are working onlookers and scouts. In the optimization function, each class has a different mission. The working bees utilize the foods, i.e., data and return the datas back to the colony. In the specified region of dance within the colony, they share this data with onlooker bees by means of dancing. The purpose of the dance is proportional to the content of nectar from the source of data, which is only utilized by the dancing bee. The onlooker bees wait for data in the colony and watch the dance of bees by working inside the colony to pick a data source. Thus, superior data source attracts more onlooker bees than poor ones. Whenever a data source is completely used, all the related working bees leave the data source and become scouts. Scout bees are looking for new sources of data. ABC algorithm's flowchart is indicated in Fig. 6.

The steps of the ABC algorithm are,

Step 1: For all working Bees, initially, the sources of food can be produced

Step 2: Restore upcoming things, which are given below,

- Every working bee leaves a source of data and finds a source of neighbor, then calculates the value of nectar and dances in the colony.
- Ach onlooker will watch the working bees dance, and depending on the dances, they select one of their data sources and then return it to that data source. The nectar value is calculated after selecting a neighbor around it.
- The abandoned data sources are found and replaced with new data that scouts identify.
- Memorized the finest source of data.

Step 3: Until (meets the specifications).

By this algorithm, the parameters of the PI controller are tuned, and the link voltage is maintained. ABC algorithm has maximum peak overshoot problems, and the CSO algorithm is utilized to overcome these disadvantages.

4.3. Chicken Swarm Optimization

To overcome the drawbacks of the maximum peak overshoot problem, the CSO algorithm is used, which is also used to tune PI parameters. The hierarchical order and individual foraging performances are imitated by means of the CSO algorithm, and the chickens are split into several parts. Each part contains 1 rooster, several hens and chicks, and each individual defines their own location according to the law of motion. Before forage, an individual with greater fitness and superior location will be obtained. The CSO algorithm is explained as,

- Split the individuals into several parts, with 1 rooster, several hens and chicks in each part.
- The finest fitness individuals are formed as roosters among the chicks; each rooster is the leader of a particular part. The chicks and hens are formed as individuals with poor fitness. Thus, hens select a part randomly, and the relations among hens and chicks are also random.
- The dominance and the relations among hens and chicks are not to be modified until its iteration reaches a certain value so that the chicken hierarchy is established.
- Individuals will forage around the rooster in each part and prevent the other individuals from being deprived of food. In order to find food, each chick will obey their mother hen and believe that the chicks will take food from other individuals. The finest advantage is held by individuals who have the leading location, and they will find food before other individuals. Every individual in the population is an effective solution to the optimization issues.

Let the population be represented as N, the percentage of the rooster be denoted as rN, the population of hen be specified as hN; the total mother hen proportion is denoted as mN, the reconstruction factor of chickens is denoted as G, the position of i^{th} individual in j^{th}dimension space is denoted as $x_{ij}(t)$.

Rooster's finest individual in the population and its update equation is expressed as,

$$\mathrm{x_{ij}(t+1) = x_{ij}(t).\left(1 + randn(0\sigma^2)\right)} \tag{35}$$

$$\sigma^2 = \begin{cases} 1, & \text{if } \mathrm{f_i \le f_a} \\ \exp\left(\frac{(\mathrm{f_a - f_i})}{|\mathrm{f_i}| + \varepsilon}\right), & \text{else} \end{cases} \qquad \mathrm{a = [1, \ldots N],\quad a \neq i} \tag{36}$$

Where the i^{th} rooster in j^{th}dimension space is denoted as $x_{ij}(t)$, $randn(0, \sigma^2)$ denotes the Gaussian distribution whose mean value is 0 and the standard deviation is σ^2, current individual for fitness is denoted as f_i, randomly chosen fitness of roosters is denoted as f_a, ε denotes constant, and its value is so small.

The updated equation of hen is expressed as

$$\mathrm{x_{ij}(t+1) = x_{ij}(t) + C_1.rand.\left(x_{r_1}j(t) - x_{ij}j(t)\right) + C_2.rand.\left(x_{r_2}j(t) - x_{ij}j(t)\right)} \tag{37}$$

$$\mathrm{C_1 = \exp\left(\left(f_i + f_{r_1}\right)/(abs(f_i) + \varepsilon)\right)} \tag{38}$$

$$C_2 = exp\left(f_{r_2} - f_i\right) r_1 \in [1, \ldots, N], r_1 \neq r_2 \neq i \tag{39}$$

Where is the location of i^{th} hen in j^{th}dimension space is denoted as $x_{ij}(t)$, $C_1 and\ C_2$denotes learning factor, $rand$ denotes constant of random, and its range is [0,1], location of the rooster, which is followed by hens, denotes $x_{r_1}j(t)$,

location of any individuals except current hen denotes $x_{r_2}j(t)$, the fitness of the rooster, which is followed by hens, denotes f_{r_1}, the fitness of any individual except i^{th} hen denotes f_{r_2}, index of the rooster, which is followed by a hen, denotes r_1, index of any individuals except i^{th} hen denotes r_2,

The update equation for the chick is expressed as,

$$x_{ij}(t+1) = x_{ij}(t) + F.\left(x_{mj}(t) - x_{ij}(t)\right) m \in [1,\ldots,N], m \neq i \quad (40)$$

Where is the location of i^{th} chick in j^{th}dimension space is denoted as $x_{ij}(t)$, coefficient of chicks denoted as F, and its range is [0,2], location of hens that is followed by chicks is denoted as $x_{mj}(t)$.

In comparison to all three optimization approaches, the CS optimization detects optimized objective function values with improved precision when compared to other approaches. This facilitates the robust functioning of the system, thereby effectively mitigating harmonics. While considering the settling time parameters, PSO and ABC generate reduced settling time when compared to CS optimization. However, the issue of maximum peak overshoot is tackled by CS optimization, whereas these issues occur in PSO and ABC approaches.

By this algorithm, the parameters of the PI controller have been tuned, and the link voltage is maintained. The converter output voltage is given to the single-phase VSI and grid.

5. PI-Controlled PWM Generator

The PI controller shown in Fig.7 is instrumental in maintaining the system stability by effectively minimizing overshoot and steady-state error. On the converter side, the error is obtained by comparing an actual voltage. V_{act} of SBQZS to the desired reference value V_{ref}, is injected into the PI controller. The K_p and K_i parameters are tuned by optimization approaches. The control signal attained from the PI controller assists the PWM generator in generating pulses that control the SBQZS converter's working [26]. On the grid side, the PI controller, in addition to the PWM generator, is exploited to control the switching operation of 1φ inverter.

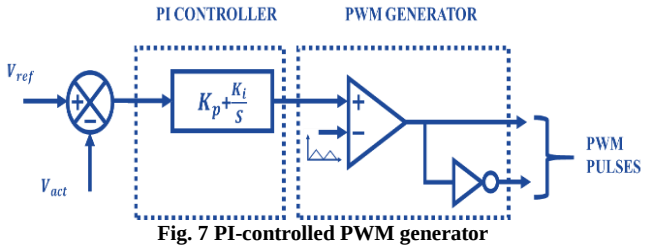

Fig. 7 PI-controlled PWM generator

6. Single-phase VSI and Grid

The attained output of the SBQZS converter, therefore, is DC-bus voltage, and it is essential to transform DC into AC to synchronize it with the grid; for that, a single-phase VSI is important. The illustration of 1Φ VSI is depicted in Fig. 8. The switches S_1 and $\overline{S_2}$ are in ON state during the positive half-cycle, whereas switches $S_2$and $\overline{S_1}$ are in ON state during the negative half-cycle at the first phase. Similarly, the arrangement is the same for the other two phases, and a filter is used to degrade current harmonics.

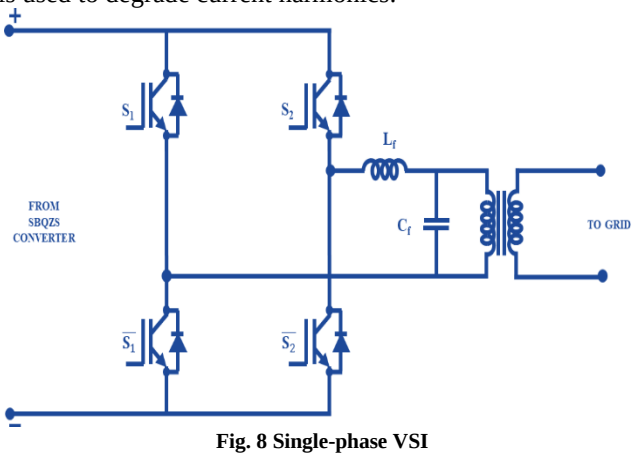

Fig. 8 Single-phase VSI

Table 1 Simulation parameters

Parameters	Values
PV panel	
Power, number of panels	200W, 5
Power, number of panels	100W, 5
Converter	
Power	1500W
Input voltage	80V
Input current	18.75A
L_1, L_2	2.2mH
C_1, C_2, C_3	570μF
C_0	1000μF
Switching frequency	10KHz
Controller	Spartan 6E FPGA
Switch	IRF840

It is important to synchronize the converter setup with the grid, and maintenance must be taken in case of imbalanced power.

Therefore, the PI controller brings up the compensation of power, thus producing essential pulses for 1Φ VSI so that power compensation is attained and synchronization of the grid is accomplished.

7. Results and Discussions

This research investigates a grid-coupled PV system WITH an SBQZS converter, where PI controller parameters are fine-tuned using PSO, ABC, and CS algorithms.

Additionally, a PI controller is employed to address grid-side imbalances. The proposed configuration is analyzed in MATLAB, and results have been obtained using the parameters listed in Table 1.

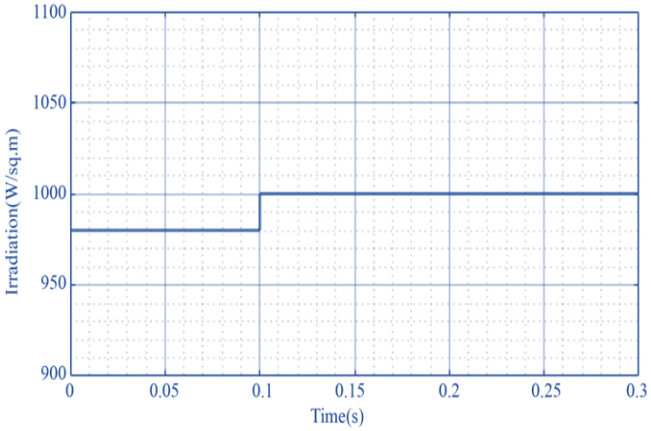

(a)

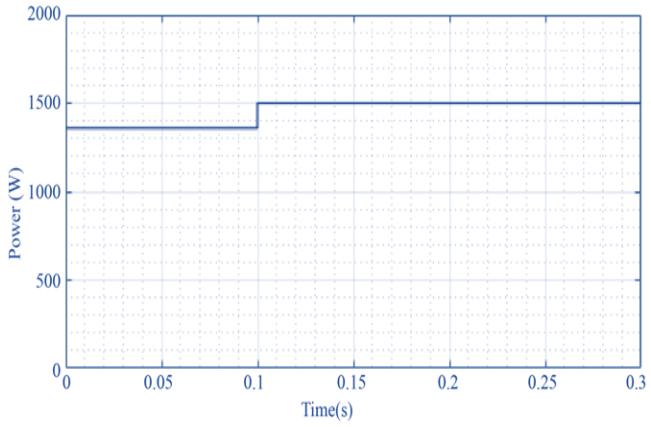

(b)

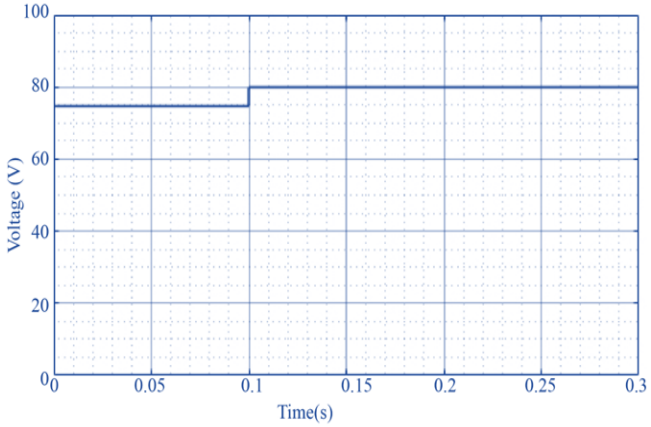

(c)

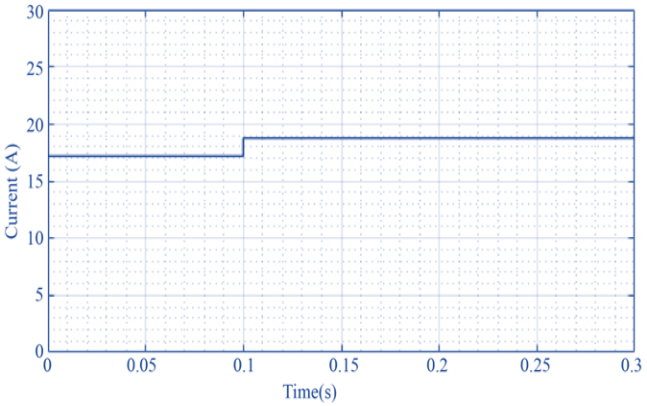

(d)

Fig. 9 (a) Solar irradiation waveform (b) Output (c) Voltage of PV (d) PV Current

Fig. 9(a) shows the solar parameters during the test period. Initially, the irradiation is $980W/m^2$, gradually increasing to $1000\,W/m^2$ after 0.1 seconds. In correspondence, the PV system current and voltage outcome is demonstrated in Fig. 9(b) and 9(c). At the beginning stage, the voltage is maintained at $78V$; after owing to a rise in temperature, the voltage rises and sustains at $80V$. Similarly, the PV current is $17.3A$, at the beginning; after $0.1s$, a step rise occurs and maintains at $18.7A$. Similarly, the solar panel's output power is initially maintained at 1360W; after 0.1s, the power is raised to 1600 Watts and sustained constant further, as described in Fig. 9(d).

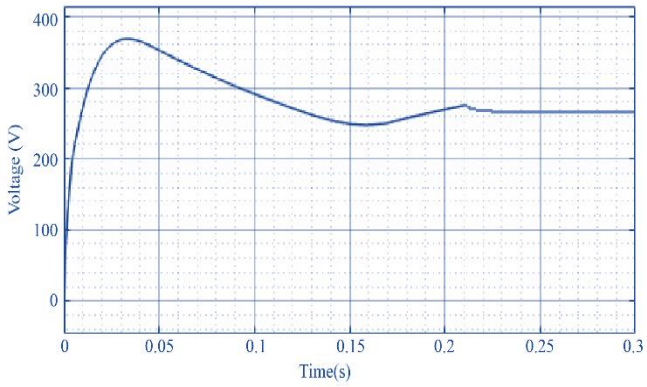

(a)

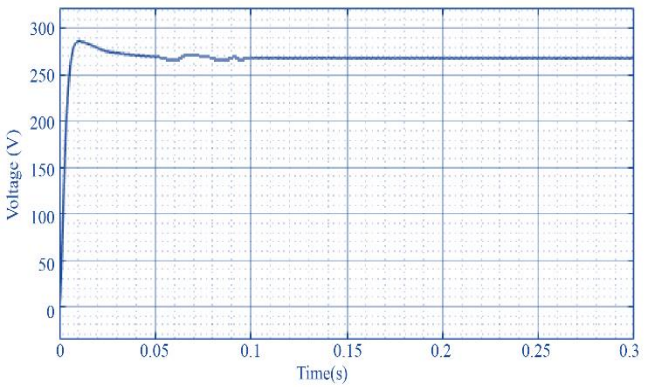

(b)

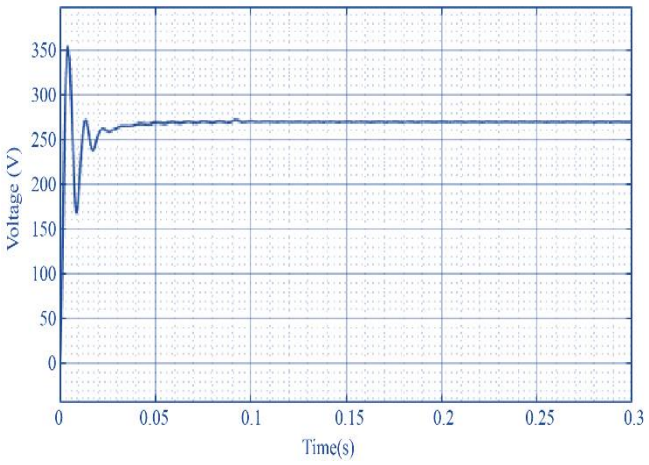

(c)

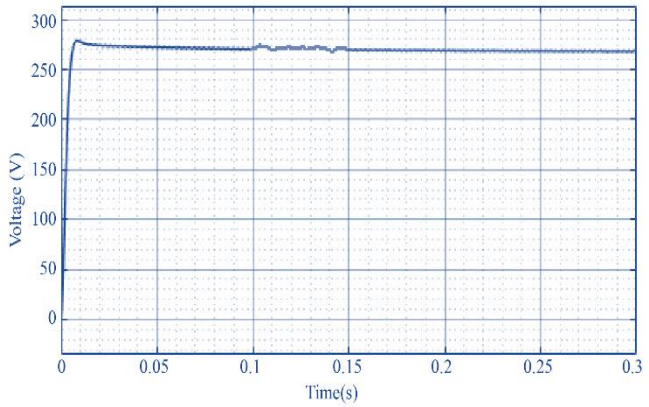

(d)

Fig. 10 Proposed SBQZS converter output voltage waveform with the (a) PI controller, (b) PSO, (c) ABC, (d) CS algorithms

The outcome of PV is fed to the SBQZS converter, and control is achieved by means of optimization algorithms. As seen in Fig. 10(a), the maximum voltage of 270V is achieved with severe peak overshoot and shows slow convergence at 0.21s. Therefore, optimization approaches are adopted to tune the parameters of the PI controller.

Consequently, optimization algorithms such as PSO, ABC and CS algorithms are incorporated in the proposed work. From Fig. 10(b) and 10(c), using PSO-PI and ABC-PI controller, a maximum voltage of 270V is attained at 0.1s, with peak overshoot. Whereas in Fig. 10(d), the CS-PI controller is adapted, which shows convergence at 0.14s.

The PSO-PI and ABC-PI controllers show faster convergence than the CS-PI controller. However, the problem of maximum peak overshoot is eliminated while the other algorithm shows maximum peak overshoot.

With the use of an effective control algorithm together with the advanced controller, the grid's voltage and frequency are maintained within acceptable ranges, even during varying loads and conditions. As a result, effective grid synchronization is achieved. Fig. 11(a) and 11(b) revealed the voltage and current waveform of single-phase VSI. It is noted that a stabilized voltage and current value is achieved, ensuring a steady electricity supply.

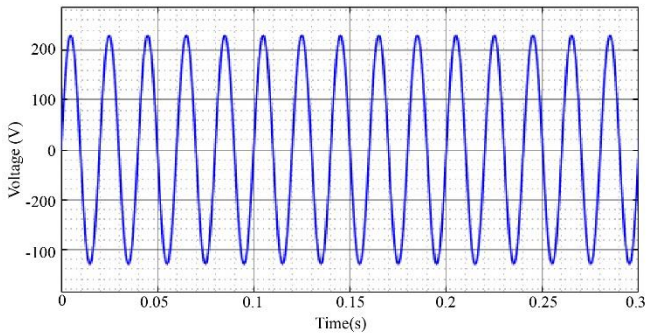

(a)

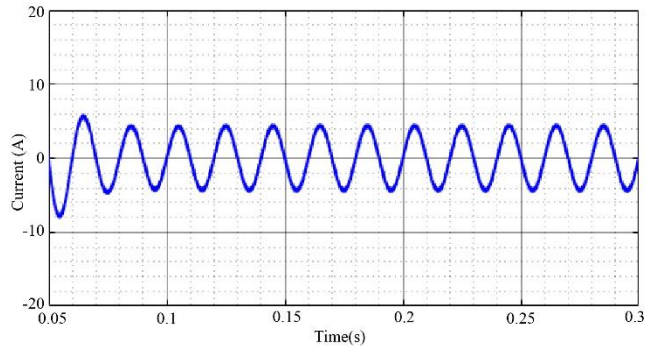

(b)

Fig. 11 Grid parameters (a) Voltage representation (b) Current representation

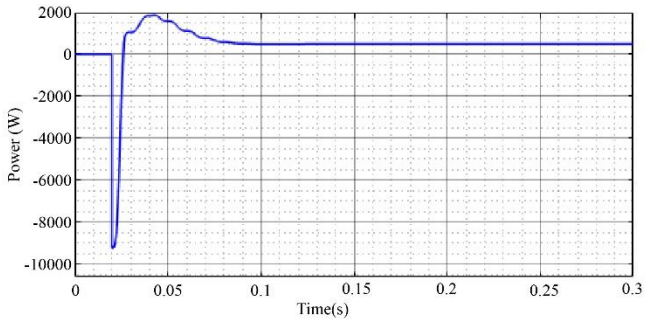

(a)

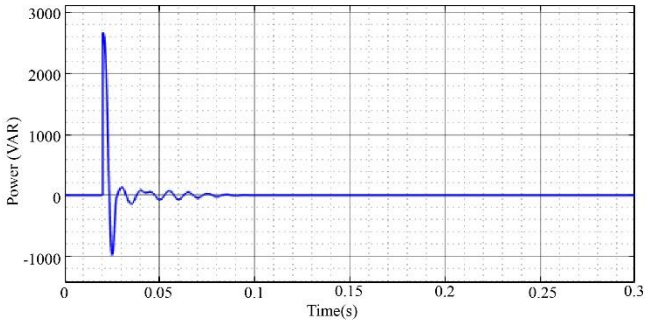

(b)

Fig. 12 (a) Real power representation, (b) Reactive power representation

Figures 12(a) and 12(b) denote the real and complex power representation. The real power waveform represents the actual power transferred to a load and is proportional to the voltage and current in phase. It appears as a continuous waveform with no phase shift. The reactive power waveform indicates oscillations at the beginning owing to the phase difference between voltage and current and later remains constants. As a consequence, the proposed system achieved optimal power flow.

The current THD outcomes of various controller responsible for optimal system performance is proved in Fig.13. It is detected that the PI controller results in a THD value of 4.9%, while Fig. 13(b) and 13(c) demonstrate the PSO-PI and ABC-PI controller THD values, which are 3.6% and 2.8%. Moreover, Fig. 13(d) showcases the THD value of the CS-PI controller, which is 1.2%. Lower THD values are generally preferable, indicating less distortion and better system quality. The CS-PI controller seems to have the lowest THD value, demonstrating that it is most effective in minimizing harmonic distortion among the listed controllers.

7.1. Hardware Analysis

The experimental setup in Fig. 14 involves a PV grid-tied system with an FPGA Spartan-6E microcontroller. The microcontroller controls and monitors tasks, ensuring the efficient integration of PV power into the grid while maintaining stability and synchronization. The FPGA Spartan-6E is a type of Field Programmable Gate Array (FPGA) from Xilinx. It is a versatile digital device programmed to perform the controlling task.

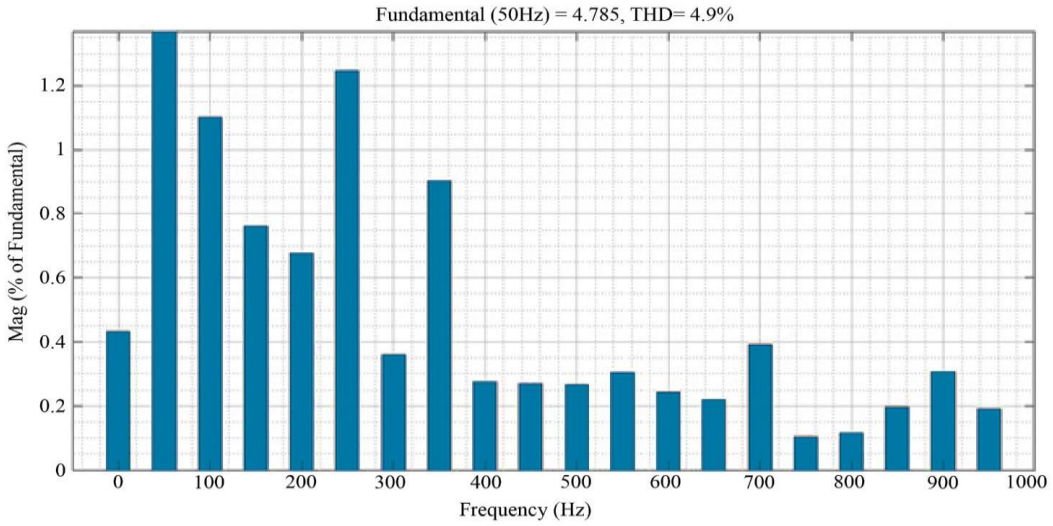

(a)

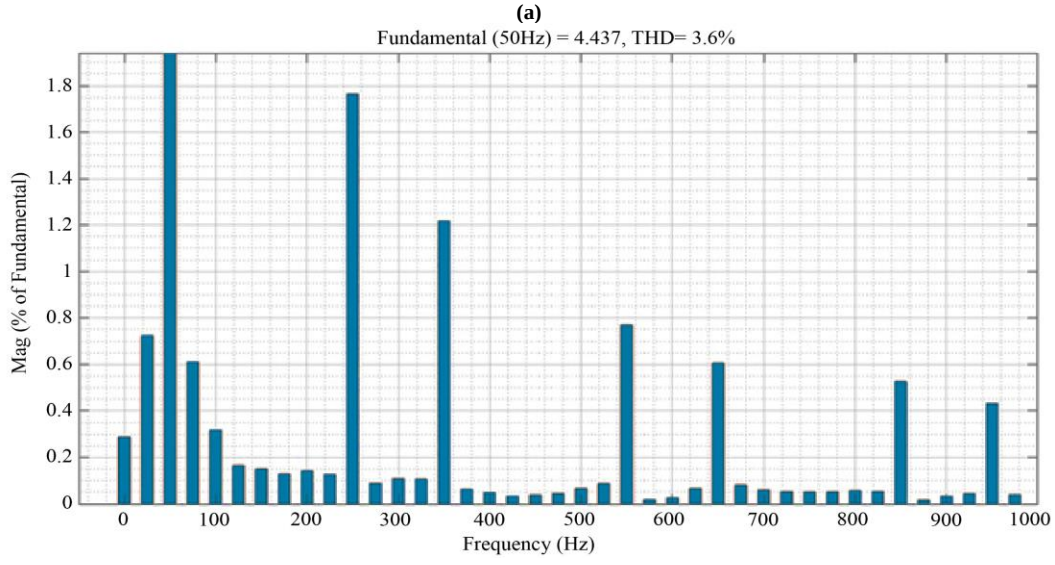

(b)

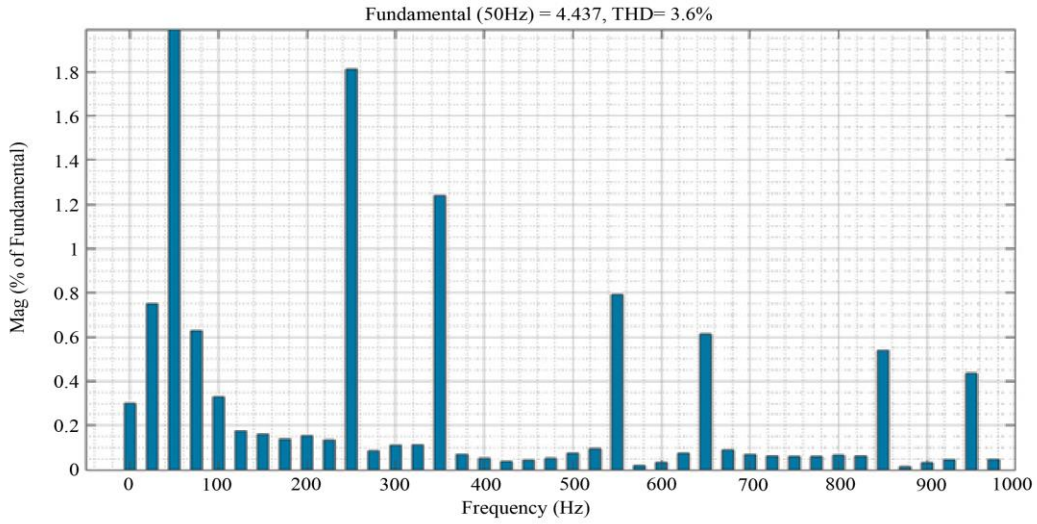

(c)

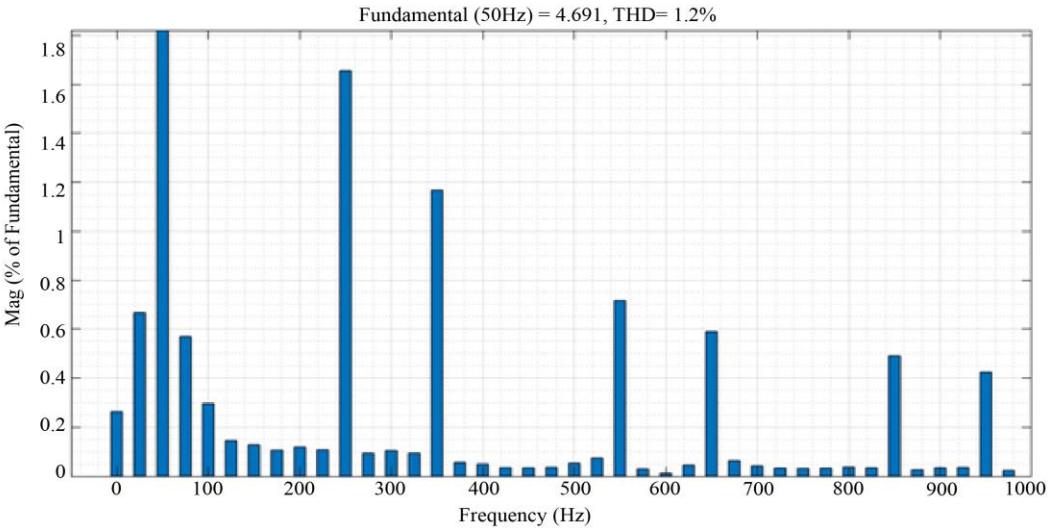

(d)

Fig. 13 Source THD using (a) PI controller, (b) PSO algorithm, (c) ABC algorithm, (d) CS algorithm

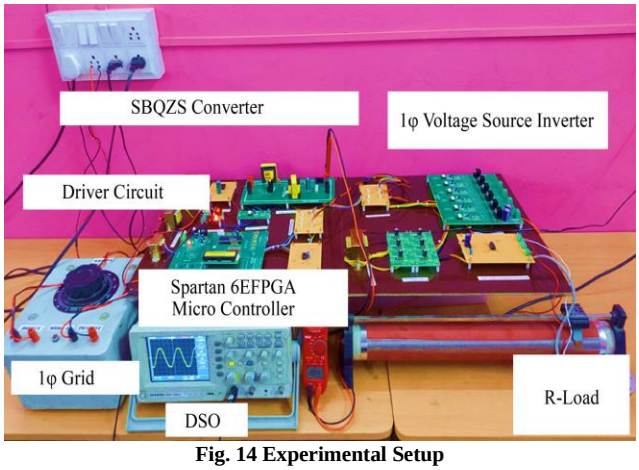

Fig. 14 Experimental Setup

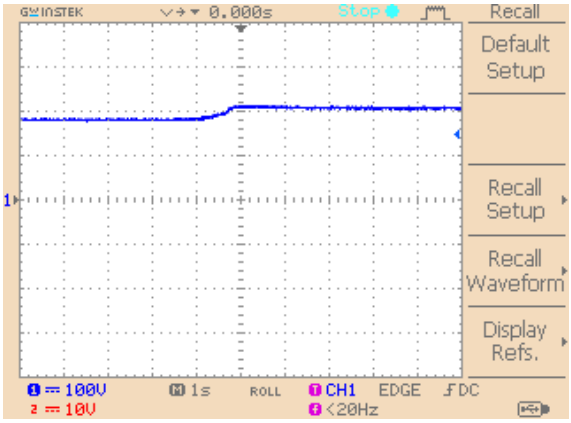

Fig. 15 PV voltage

The waveform representing solar PV voltage is depicted in Fig. 15, which shows that the voltage rises from a gradual level of 28V to 30V, with slight oscillation. The oscillation is due to the change in temperature and irradiance level of the PV panel.

The converter output voltage obtained by utilized the optimization algorithm for tuning the PI controller is depicted in Fig. 16. It is noticed that all three optimization algorithms achieve a maximum output voltage of 30V, but utilizing PSO-PI and ABC-PI, shows faster convergence, as shown in Fig. 16(a) and 16(b), with high peak overshoot. While the CS-PI controller converges later, as depicted in Fig. 16 (d), with the elimination of the peak overshoot issue.

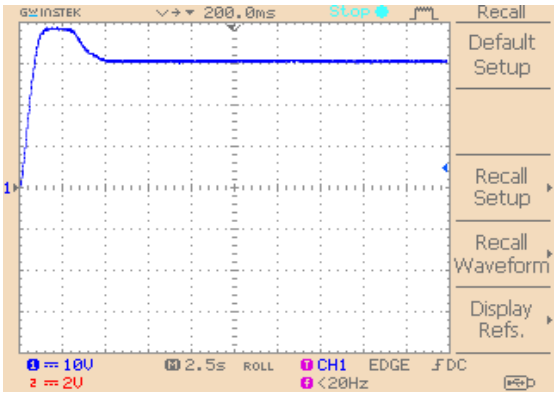

(a)

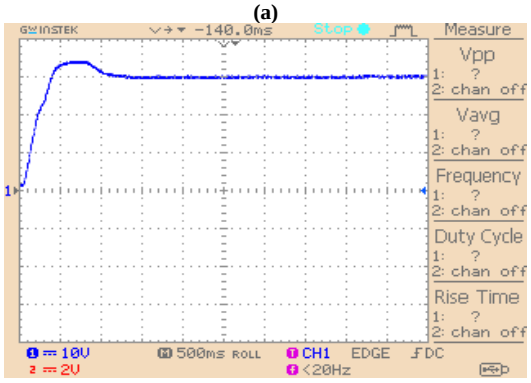

(b)

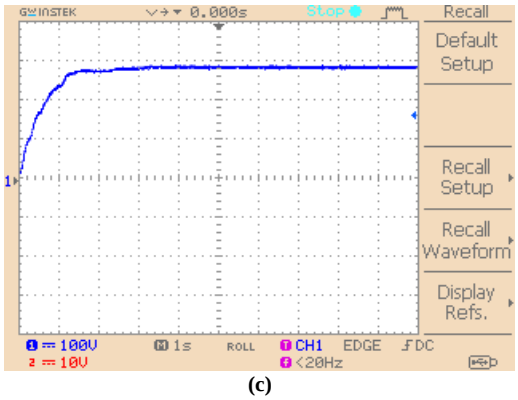

(c)

Fig. 16 Converter control using (a) PSO-PI, (b) ABC-PI and (c) CS-PI Controller

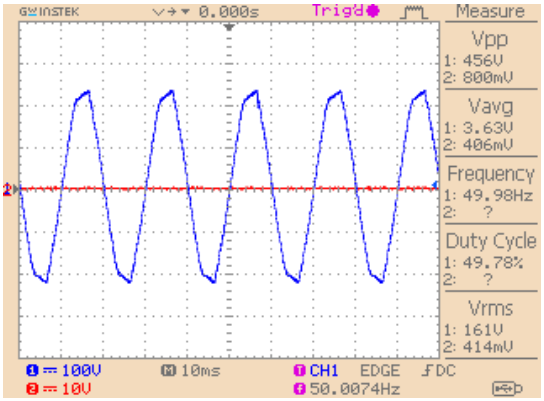

(a)

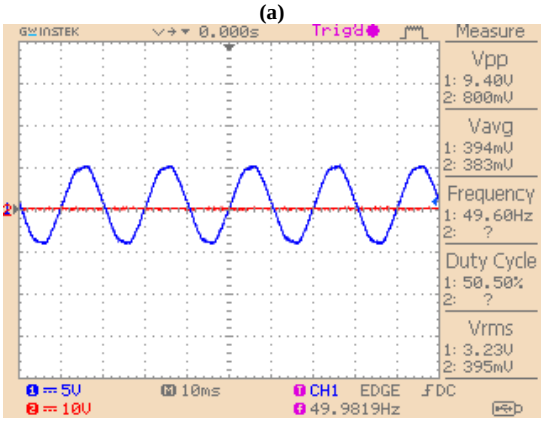

(b)

Fig. 17(a) Grid Voltage and (b) Grid Current

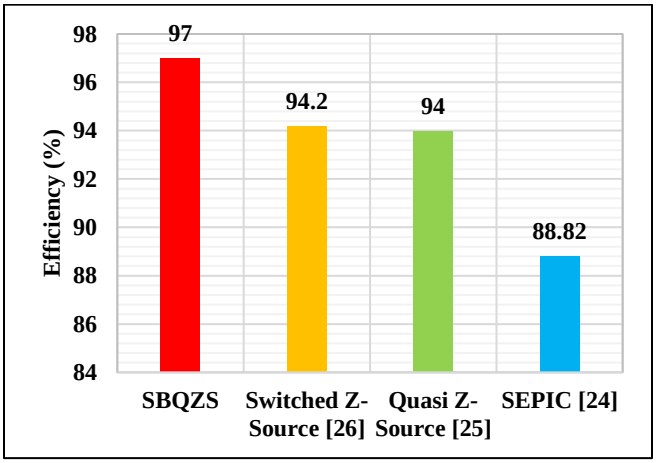

Fig. 18 Comparison of efficiency

The grid voltage and current waveforms depicted in Fig. 17(a) and 17(b) remain steady without oscillation, ensuring a consistent and reliable power supply. This stability is crucial for the efficient operation of connected devices and prevents disturbances in the electrical grid.

A detailed comparison is executed by comparing the working of the proposed configuration related efficiency, voltage gain and THD.

Fig. 18 illustrates the comparison of efficiency for different converters and reveals that the SEPIC converter [27] attains 88.82% efficiency, whereas Quasi Z-Source [28] and Switched Z-Source [29] achieve 94% and 94.2%, respectively. In contrast, the proposed SBQZS converter results in a maximum efficiency of 97%, which is comparatively high.

Fig. 19 illustrates the comparison of voltage gain for existing converters, and it is revealed that the voltage-gain ratio for the boost converter is 1:1.5, whereas 1:2 for Z-source, 1:8 for SEPIC and proposed SBQZS is 1:10, which is comparatively high.

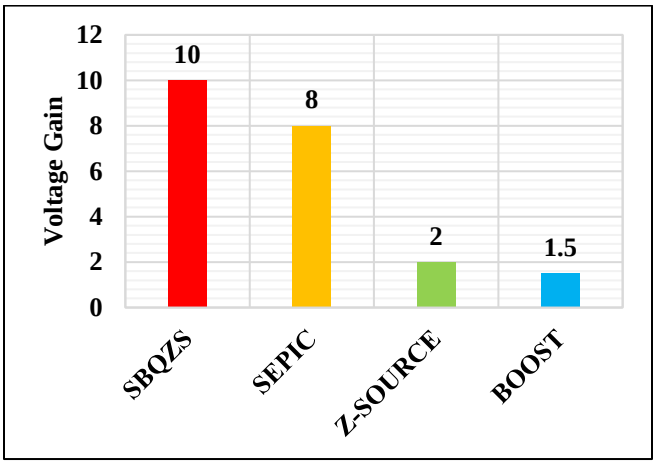

Fig. 19 Comparison of voltage gain

Fig. 20 illustrates the comparative analysis of THD with different algorithms, and it is revealed that by the PI controller, THD of 4.9% is attained; by the PSO algorithm, THD of 3.6% is attained; by the ABC algorithm, THD of 2.8% is attained; by CS algorithm, THD of 1.2% is attained which is generally considered to be quite low.

Table 2. Settling time of the proposed configuration with different algorithms

Settling Time	PI controller	PSO algorithm	ABC algorithm	CS algorithm
	0.21 *s*	0.1 *s*	0.1 *s*	0.14 *s*

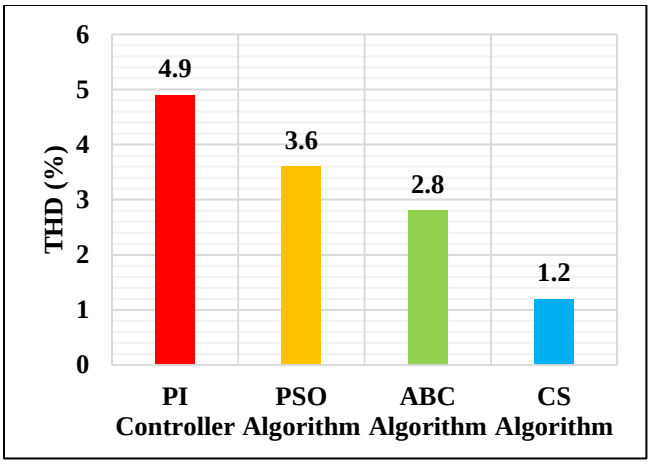

Fig. 20 Comparison of Current THD

Table 2 demonstrates the settling time of the proposed configuration with different algorithms. It is revealed that with the PI controller, the settling time is 0.21 seconds; with PSO and ABC algorithms, the settling time is 0.1 seconds; with the CS algorithm, the settling time is 0.14 seconds.

8. Conclusion

Grid integration of the PV system is scrutinized with the SBQZS converter in this work. A high gain converter with a maximum voltage gain of 1:10 is proposed, enhancing PV voltage to 270V. The converter exhibits less stress across the components correspondingly. The controlling of the converter is accomplished with a PI controller whose parameters are tuned with PSO, ABC and CS algorithms. Both the PSO and ABC approach generate a settling time of 0.1s, while the settling time of the CS approach is 0.14s. Some inequities affect the overall system performance while synchronizing the PV system with the grid. A PI controller is included in the grid side by which the reactive power compensation is accomplished. The validation of the proposed configuration is executed in MATLAB simulation. It is perceived that the SBQZS converter generates an efficiency of 97%. The PSO, ABC and CS approaches generate a THD of 3.6%, 2.8% and 1.2%, respectively. Future works can concentrate on the bidirectional operation of the converter in grid-associated PV systems.

References

[1] Subhendu Dutta, and Kishore Chatterjee, "A Buck and Boost Based Grid Connected PV Inverter Maximizing Power Yield from Two PV Arrays in Mismatched Environmental Conditions," *IEEE Transactions on Industrial Electronics*, vol. 65, no. 7, pp. 5561–5571, 2018. [CrossRef] [Google Scholar] [Publisher Link]

[2] Nishant Kumar, Bhim Singh, and Bijaya Ketan Panigrahi, "Framework of Gradient Descent Least Squares Regression-Based NN Structure for Power Quality Improvement in PV-Integrated Low-Voltage Weak Grid System," *IEEE Transactions on Industrial Electronics*, vol. 66, no. 12, pp. 9724–9733, 2019. [CrossRef] [Google Scholar] [Publisher Link]

[3] Sara Yazdani et al., "Advanced Current-Limiting and Power-Sharing Control in a PV-Based Grid-Forming Inverter under Unbalanced Grid Conditions," *IEEE Journal of Emerging and Selected Topics in Power Electronics*, vol. 8, no. 2, pp. 1084–1096, 2020. [CrossRef] [Google Scholar] [Publisher Link]

[4] Nishant Kumar et al., "Leaky-Least-Logarithmic-Absolute-Difference-Based Control Algorithm and Learning-Based InC MPPT Technique for Grid-Integrated PV System," *IEEE Transactions on Industrial Electronics*, vol. 66, no. 11, pp. 9003–9012, 2019.

[CrossRef] [Google Scholar] [Publisher Link]

[5] Nishant Kumar et al., "Implementation of Multilayer Fifth-Order Generalized Integrator-Based Adaptive Control for Grid-Tied Solar PV Energy Conversion System," *IEEE Transactions on Industrial Informatics*, vol. 14, no. 7, pp. 2857–2868, 2018. [CrossRef] [Google Scholar] [Publisher Link]

[6] Nasif Mahmud, Ahmad Zahedi, and Asif Mahmud, "A Cooperative Operation of Novel PV Inverter Control Scheme and Storage Energy Management System Based on ANFIS for Voltage Regulation of Grid-Tied PV System," *IEEE Transactions on Industrial Informatics*, vol. 13, no. 5, pp. 2657–2668, 2017. [CrossRef] [Google Scholar] [Publisher Link]

[7] Shailendra Kumar, and Bhim Singh, "Self-Normalized-Estimator-Based Control for Power Management in Residential Grid Synchronized PV-BES Microgrid," *IEEE Transactions on Industrial Informatics*, vol. 15, no. 8, pp. 4764–4774, 2019. [CrossRef] [Google Scholar] [Publisher Link]

[8] R. K. Negesh et al., "Implementation of PV-Wind based Microgrid System using Whale Optimization Algorithm," *SSRG International Journal of Electrical and Electronics Engineering*, vol. 10, no. 4, pp. 12-23, 2023. [CrossRef] [Google Scholar] [Publisher Link]

[9] Shouxiang Wang et al., "Interval Overvoltage Risk Based PV Hosting Capacity Evaluation Considering PV and Load Uncertainties," *IEEE Transactions on Smart Grid*, vol. 11, no. 3, pp. 2709–2721, 2020. [CrossRef] [Google Scholar] [Publisher Link]

[10] Nishant Kumar et al., "Integration of Solar PV With Low-Voltage Weak Grid System: Using Normalized Laplacian Kernel Adaptive Kalman Filter and Learning Based InC Algorithm," *IEEE Transactions on Power Electronics*, vol. 34, no. 11, pp. 10746–10758, 2019. [CrossRef] [Google Scholar] [Publisher Link]

[11] Daiki Yamaguchi, and Hideaki Fujita, "A New PV Converter for a High-Leg Delta Transformer Using Cooperative Control of Boost Converters and Inverters," *IEEE Transactions on Power Electronics*, vol. 33, no. 11, pp. 9542–9550, 2018. [CrossRef] [Google Scholar] [Publisher Link]

[12] Balaji Chandrasekar et al., "Non-Isolated High-Gain Triple Port DC–DC Buck-Boost Converter with Positive Output Voltage for Photovoltaic Applications," *IEEE Access*, vol. 8, pp. 113649–113666, 2020. [CrossRef] [Google Scholar] [Publisher Link]

[13] Kumaran Nathan et al., "A New DC–DC Converter for Photovoltaic Systems: Coupled-Inductors Combined Cuk-SEPIC Converter," *IEEE Transactions on Energy Conversion*, vol. 34, no. 1, pp. 191–201, 2019. [CrossRef] [Google Scholar] [Publisher Link]

[14] Kok Soon Tey et al., "Improved Differential Evolution-Based MPPT Algorithm Using SEPIC for PV Systems Under Partial Shading Conditions and Load Variation," *IEEE Transactions on Industrial Informatics*, vol. 14, no. 10, pp. 4322–4333, 2018. [CrossRef] [Google Scholar] [Publisher Link]

[15] Julio Cezar dos Santos de Morais, Juliano Luiz dos Santos de Morais, and Roger Gules, "Photovoltaic AC Module Based on a Cuk Converter with a Switched-Inductor Structure," *IEEE Transactions on Industrial Electronics*, vol. 66, no. 5, pp. 3881–3890, 2019. [CrossRef] [Google Scholar] [Publisher Link]

[16] S. Kaushik et al., "A Harmonic Detection for Grid Connected PV System Under Non-Linear Load using Cuk Converter," *SSRG International Journal of Electrical and Electronics Engineering*, vol. 7, no. 3, pp. 6-11, 2020. [CrossRef] [Publisher Link]

[17] Siddhartha A. Singh et al., "Modeling, Design, Control, and Implementation of a Modified Z-Source Integrated PV/Grid/EV DC Charger/Inverter," *IEEE Transactions on Industrial Electronics*, vol. 65, no. 6, pp. 5213–5220, 2018. [CrossRef] [Google Scholar] [Publisher Link]

[18] Xiaoqiang Guo et al., "Transformerless Z-Source Four-Leg PV Inverter with Leakage Current Reduction," *IEEE Transactions on Power Electronics*, vol. 34, no. 5, pp. 4343–4352, 2019. [CrossRef] [Google Scholar] [Publisher Link]

[19] D. Venkatramanan, and Vinod John, "Dynamic Modeling and Analysis of Buck Converter Based Solar PV Charge Controller for Improved MPPT Performance," *IEEE Transactions on Industry Applications*, vol. 55, no. 6, pp. 6234–6246, 2019. [CrossRef] [Google Scholar] [Publisher Link]

[20] Jubaer Ahmed, and Zainal Salam, "An Enhanced Adaptive P&O MPPT for Fast and Efficient Tracking Under Varying Environmental Conditions," *IEEE Transactions on Sustainable Energy*, vol. 9, no. 3, pp. 1487–1496, 2018. [CrossRef] [Google Scholar] [Publisher Link]

[21] J. Prasanth Ram et al., "Detection and Identification of Global Maximum Power Point Operation in Solar PV Applications Using a Hybrid ELPSO-P&O Tracking Technique," *IEEE Journal of Emerging and Selected Topics in Power Electronics*, vol. 8, no. 2, pp. 1361-1374, 2020. [CrossRef] [Google Scholar] [Publisher Link]

[22] Mohammed Alsumiri, "Residual Incremental Conductance Based Nonparametric MPPT Control for Solar Photovoltaic Energy Conversion System," *IEEE Access*, vol. 7, pp. 87901–87906, 2019. [CrossRef] [Google Scholar] [Publisher Link]

[23] Nishant Kumar et al., "Self-Adaptive Incremental Conductance Algorithm for Swift and Ripple-Free Maximum Power Harvesting from PV Array," *IEEE Transactions on Industrial Informatics*, vol. 14, no. 5, pp. 2031–2041, 2018. [CrossRef] [Google Scholar] [Publisher Link]

[24] Hegazy Rezk et al., "Design and Hardware Implementation of New Adaptive Fuzzy Logic-Based MPPT Control Method for Photovoltaic Applications," *IEEE Access*, vol. 7, pp. 106427–106438, 2019. [CrossRef] [Google Scholar] [Publisher Link]

[25] Lotfi Farah et al., “A Highly-Efficient Fuzzy-Based Controller with High Reduction Inputs and Membership Functions for a Grid-Connected Photovoltaic System,” *IEEE Access*, vol. 8, pp. 163225–163237, 2020. [CrossRef] [Google Scholar] [Publisher Link]

[26] K. Praveena, and Katragadda Swarnasri, "ANFIS Control of PV Tied Grid System with Multi-Carrier PWM-Based Modular 5-Level Converter," *SSRG International Journal of Electrical and Electronics Engineering*, vol. 9, no. 12, pp. 145-155, 2022. [CrossRef] [Publisher Link]

[27] Patan Javeed et al., "SEPIC Converter for Low Power LED Applications," *Journal of Physics: Conference Series*, vol. 1818, no. 1, 2021. [CrossRef] [Google Scholar] [Publisher Link]

[28] Anish Ahmad, R. K. Singh, and Abdul R. Beig, "Switched-Capacitor based Modified Extended High Gain Switched Boost Z-Source Inverters," *IEEE Access*, vol. 7, pp. 179918-179928, 2019. [CrossRef] [Google Scholar] [Publisher Link]

[29] Sohrab Naderi, and Hasan Rastegar, "A New Non-Isolated Active Quasi Z-Source Multilevel Inverter with High Gain Boost," *IEEE Access*, vol. 11, pp. 2941-2951, 2023. [CrossRef] [Google Scholar] [Publisher Link]